Supplementary Information for: Core-Level Binding Energy Shifts in Ultrathin Alkali-Halide Films on Metals: KCl on Ag(100)

Séverine Le Moal,[†] Ina Krieger,[‡] Roman Kremring,[‡] Simon Weiß,[¶,§] Xiaosheng Yang,[¶,§] Serguei Soubatch,[¶,§] F. Stefan Tautz,[¶,§,‖] Mathieu Silly,[⊥] Andrei G. Borisov,[†] Moritz Sokolowski,[‡] and Eric Le Moal[*,†]

†*Université Paris-Saclay, CNRS, Institut des Sciences Moléculaires d'Orsay, 91405, Orsay, France*

‡*Institut für Physikalische und Theoretische Chemie der Universität Bonn, Wegelerstrasse 12, 53115 Bonn, Germany*

¶*Peter Grünberg Institut (PGI-3), Forschungszentrum Jülich, 52425 Jülich, Germany*

§*Jülich Aachen Research Alliance (JARA)-Fundamentals of Future Information Technology, 52425 Jülich, Germany*

‖*Experimental Physics IV A, RWTH Aachen University, 52074 Aachen, Germany*

⊥*Synchrotron-SOLEIL, Saint-Aubin, BP48, F91192 Gif sur Yvette Cedex, France*

E-mail: eric.le-moal@universite-paris-saclay.fr

Phone: +33 (0)1 69 15 66 97. Fax: +33 (0)1 69 15 67 77

Additional characterization of the sample

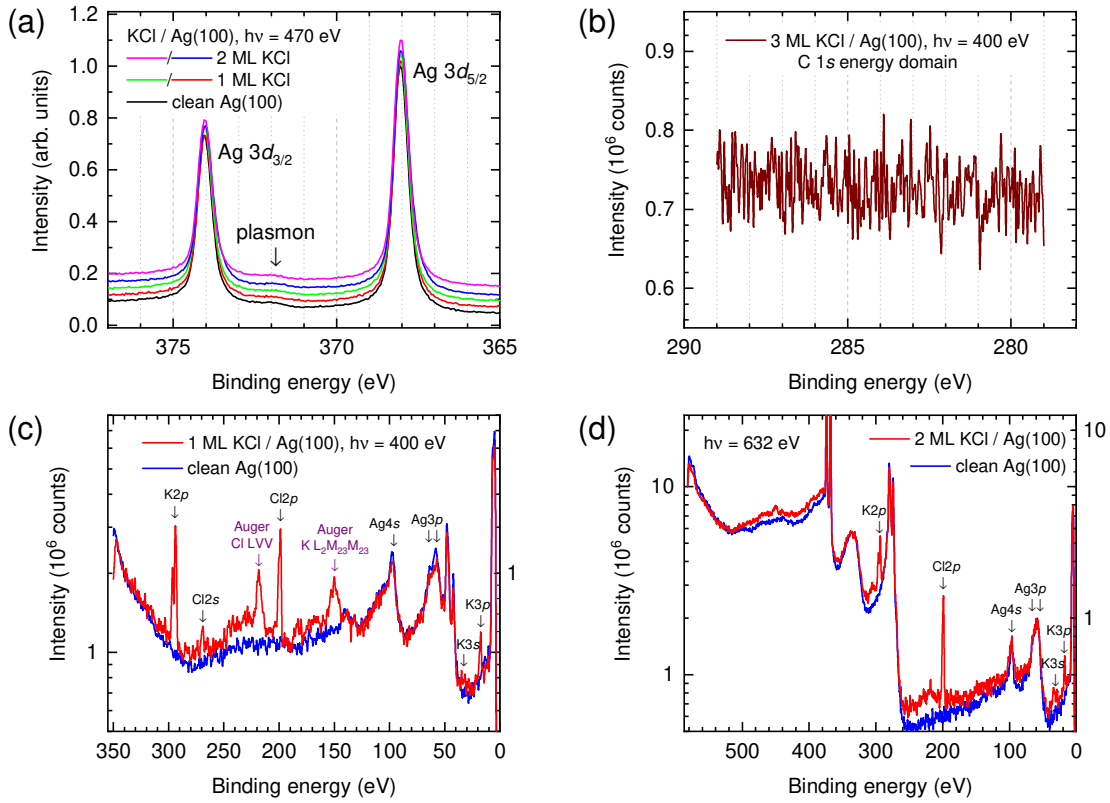

Figure S1: (a) HRPES spectra of the Ag $3d$ core-level doublet for 1 ML and 2 ML KCl films grown on Ag(100) and for clean Ag(100). The intensity maximum is normalized to unity and a small vertical offset is added to help distinguish the spectra from each other. (b) HRPES spectrum measured in the binding energy region of the C $1s$ core-level singlet for a 3 ML KCl film grown on Ag(100). (c,d) XPS survey spectra of (c) 1 ML and (d) 2 ML KCl films grown on Ag(100), compared to clean Ag(100). $h\nu$ is the photon energy. Intensity is plotted in log scale.

Figure S1(a) shows high-resolution photoemission spectra (HRPES) of the Ag $3d$ core-level doublet measured on KCl films, whose nominal thickness is either 1 or 2 ML grown on Ag(100) at room temperature, and on the clean Ag(100) substrate. As expected, we measure that the energy splitting of the Ag$3d$ core level due to spin-orbit coupling is about 6.0 eV. The shoulder on the low-energy side of the Ag $3d_{3/2}$ peak is due to energy transfer from the photoelectrons to plasmons in the substrate. We find that the center of this shoulder is shifted by about 3.8 eV upward in binding energy with respect to the Ag $3d_{5/2}$ peak, which matches the experimental value of the plasma resonance of silver available in the literature

(3.78 eV).

In the spectra shown in Fig. S1(a), we do not observe any peak or shoulder due to energy transfer from the photoelectrons to color centers, which would be centered at about 2.2 eV from the Ag $3d_{5/2}$ peak on its high-energy side. This non-observation indicates that, in the experimental conditions used, the X-ray induced degradation of 1 ML and 2 ML KCl films on Ag(100) is negligible at the time scale of the measurements. All the HRPES data that featured signs of degradation due to X-ray irradiation were discarded from this study.

Moreover, the energy position and lineshape of the Ag $3d$ core-level HRPES peaks shown in Fig. S1(a) are not modified when 1 or 2 ML of KCl is deposited on the bare Ag(100) surface. This indicates that KCl does not chemically react with Ag, i.e., the Cl $2p$ and K $2p$ electron binding energy shifts reported in the paper are not due to K-Ag or Cl-Ag covalent bonding or alloying.

Figure S1(b) shows an HRPES spectrum measured on a 3 ML KCl grown on Ag(100), in the binding energy region where the C $1s$ singlet peak is expected. The non-observation of this peak indicates the absence of any significant carbon contamination in the sample.

Figures S1(c) and S1(d) show X-ray photoemission (XPS) survey samples recorded for 1 ML and 2 ML KCl films on Ag(100) and for the clean Ag(100) substrate. The XPS and Auger peaks are assigned to silver, chlorine and potassium. No other peaks can be distinguished from the noise background, which confirms the absence of any significant contamination of the sample and of the preparations used in this study.

Additional information about the NIXSW measurements

Using a fitting model based on the parameters (widths, positions, and the area ratio) of the lines constituting the two doublets fitted to the spectra shown in Fig. 3 in the article, we determine the respective yield curves as a function of the photon energy for both components. Figure S2 shows examples of these photoemission yield curves. When the photon energy is

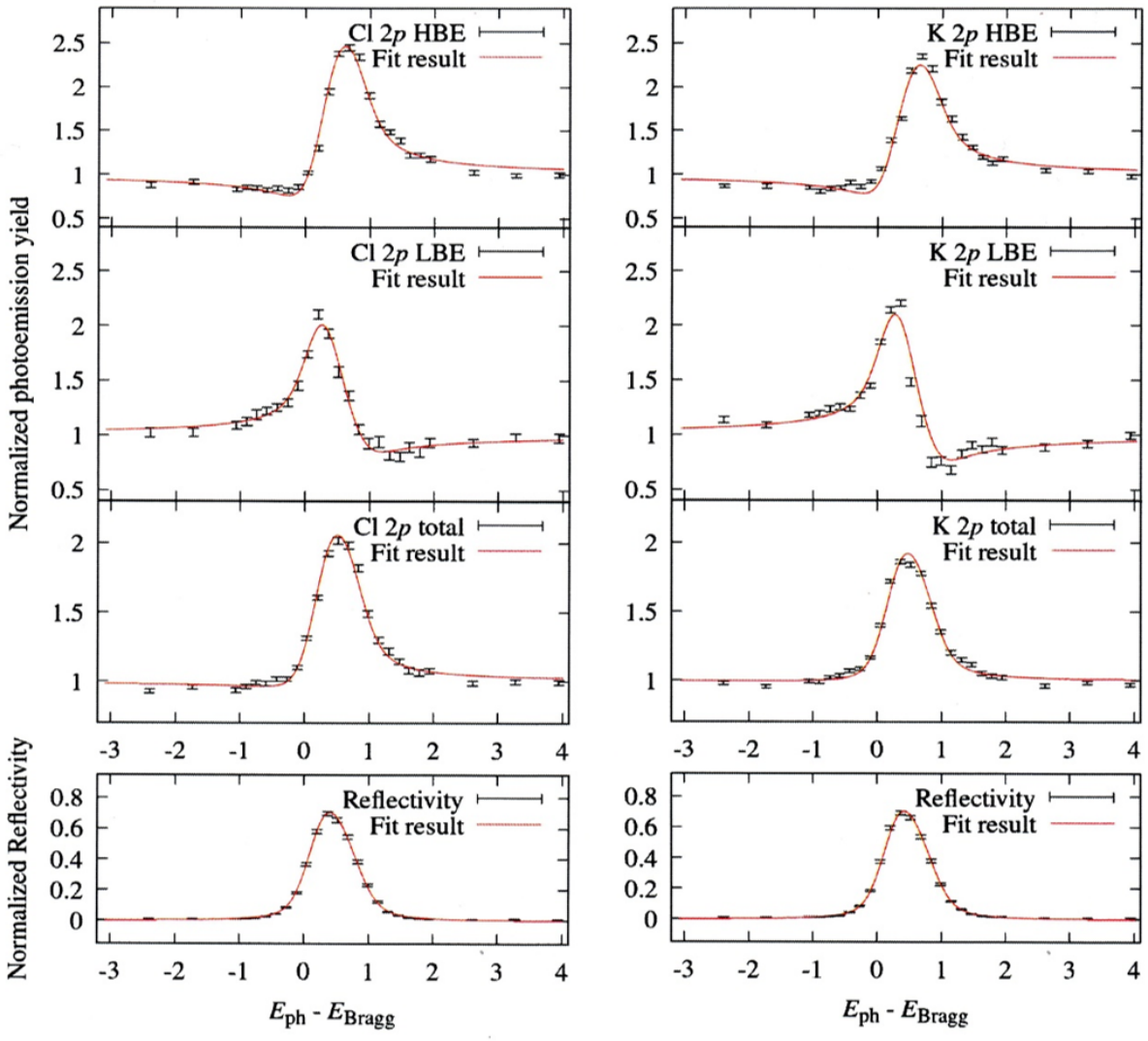

Figure S2: Photoelectron yield curves of the HBE and LBE components and the total intensities of the 2*p* lines of Cl and K. In addition the reflectivities are shown. The red lines are fits to the data for the determination of the coherent positions and fractions.

varied around the Bragg energy, the intensities of the LBE and HBE components change. However, the peak of the photoemission yield curve is not observed at the same photon energy for the LBE and HBE components. This reveals that the LBE and HBE components stem from K and Cl atoms that are at different vertical heights.

Figure S2 also shows the integrated intensities of the lines, which are computed from the respective integrals over the emission lines. In the Argand diagram shown in Fig. 3(c) of the article, the coherent fractions of the Argand vectors of the integrated intensities are comparatively small (~ 0.2 – 0.3) for the K2p and the Cl2p lines. This is an effect of the KCl layer spacing of 3.15 Å that corresponds to $1.54 \times d_{\mathrm{Ag}(200)}$. It causes that the Argand vectors of the components of the first and second layer point into almost opposite directions in the Argand diagram (at an angle of $\sim 40\% \cdot 2\,\pi$ to each other). According to the "lever rule", the Argand vector of the integrated signal corresponds to the sum of the two Argand vectors of the HBE and LBE components weighted by the molar fractions of the species. As a result, Argand vector of the integrated signal becomes small and its coherent fraction, f_{c} is close to zero, as seen in Fig. 3(c) of the article.

Additional calculations

Figure S3 shows the effect of varying the vertical positions of the Cl^- and K^+ ions of the first atomic layer (at the KCl/Ag interface) on the calculated binding energy shifts relative to the first atomic layer. The crosses indicate the vertical positions used in the calculations and the uncertainty on these positions (± 0.02 Å). Fig. S3 is to be compared to Fig. 4 of the article. In Fig. 4, the vertical positions of the ions of the second atomic layer (at the KCl/vacuum interface) are kept constant. In Fig. S3, the vertical positions of the ions of the second atomic layer are also changed and the vertical distances between the ions of the two atomic layers are kept constant. Similar results are obtained in Fig. S3 and Fig. 4, which highlights the dominating effect of the vertical positions of the ions at the KCl/Ag interface.

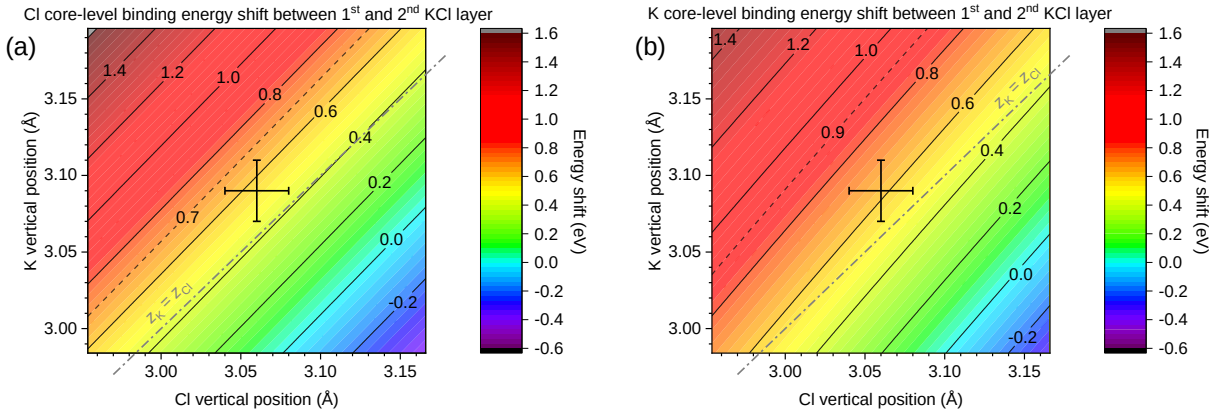

Figure S3: Theoretical core-level binding energy shifts calculated for a two atomic layer-thick KCl film on Ag(100) with the inclusion of the image charge effects. The binding energy shifts relative to the first atomic layer of the KCl film is plotted as a function of the vertical distance of the Cl^- and K^+ ions of the first atomic layer from the surface atomic plane. The vertical positions of the Cl^- and K^+ ions of the second atomic layer are also changed and the vertical distances between the ions of the two atomic layers are kept constant. The first and second atomic layers of the KCl film are the KCl layers at the KCl/Ag and KCl/vacuum interfaces, respectively. The crosses at the center of the graphs indicate the vertical positions (d_c) deduced from the NIXSW measurements and used in the calculations. The horizontal and vertical widths of the cross correspond to the estimated maximal uncertainty on d_c, i.e., ± 0.02 Å.